

# RSC Advances



This is an *Accepted Manuscript*, which has been through the Royal Society of Chemistry peer review process and has been accepted for publication.

*Accepted Manuscripts* are published online shortly after acceptance, before technical editing, formatting and proof reading. Using this free service, authors can make their results available to the community, in citable form, before we publish the edited article. This *Accepted Manuscript* will be replaced by the edited, formatted and paginated article as soon as this is available.

You can find more information about *Accepted Manuscripts* in the [Information for Authors](#).

Please note that technical editing may introduce minor changes to the text and/or graphics, which may alter content. The journal's standard [Terms & Conditions](#) and the [Ethical guidelines](#) still apply. In no event shall the Royal Society of Chemistry be held responsible for any errors or omissions in this *Accepted Manuscript* or any consequences arising from the use of any information it contains.

**Construction of bone-like surface layer on hydroxyl-modified carbon/carbon composite implants *via* biomimetic mineralization and *in vivo* test**

Ning Cao<sup>a\*</sup>, Zhenguo Yang<sup>b</sup>, Bai Yang<sup>a</sup>, Wenbo Wang<sup>b</sup>, Rabah Boukherroub<sup>c</sup>, Musen Li<sup>d</sup>

<sup>a</sup> *College of Mechanical and Electrical Engineering, China University of Petroleum, Qingdao 266580, P.R. China*

<sup>b</sup> *The Second Affiliated Hospital, Shandong University of Chinese Traditional Medicine, Ji'nan 250001, P.R. China*

<sup>c</sup> *Institut d'Electronique, de Microélectronique et de Nanotechnologie (IEMN), UMR CNRS8520, Université Lille1, Avenue Poincaré – BP60069, 59652 Villeneuve d'Ascq, France*

<sup>d</sup> *Key Laboratory for Liquid-Solid Structural Evolution and Processing of Materials (Ministry of Education) Shandong University, Jinan 250061, P.R. China*

\*To whom correspondence should be addressed: Ning Cao (caoning1982@gmail.com)

**Abstract**

Carbon/carbon composites, solely composed of pure carbon, are typical fiber fabric reinforced porous composites. They have been widely studied due to their excellent bio-inert performance and mechanical properties. However, their applications are restricted by two problems, i.e., easy dissociation of surface carbon particles and poor wettability of common bioactive coatings on their surface. To overcome these problems, we have adopted a biomimetic mineralization method, where Mg-doped hydroxyapatite particles were successfully prepared on hydroxyl-modified C/C surfaces, prepared *via* HNO<sub>3</sub> oxidation. In this way, the original porous morphology of C/C, which is conducive to cell proliferation, is well-preserved. In the meanwhile, the introduction of electrochemical method sped up the process of bio-mineralization and facilitated the construction of bone-like surface layers. *In vivo* test revealed that 90 days after implantation for bone defect repair, the resulted C/C displayed unprecedented surface chemical stability and biocompatibility.

**Keywords:** *Carbon fiber reinforced carbon composites; Surface oxidation; Nitric acid; Hydroxyapatite; Biomimetic mineralization*

## 1. Introduction

It is well established that almost all the hard tissues (bones and teeth, etc.) of human body are natural porous mineralized composites made of minerals, carbonated hydroxyapatite ( $\text{Ca}_{10}(\text{PO}_4)_6(\text{OH})_2$ ), collagen and water.<sup>1</sup> When a tissue defect cannot be naturally healed, a proper scaffold material has to be used to repair it. After that, the regenerated osseous tissue will, guided by the scaffold, achieve tissue reconstruction through bio-mineralization process.<sup>2</sup> Therefore, to ensure successful tissue reconstruction with osteoblasts and osteoclasts, it is essential for the scaffold to have excellent biocompatibility.

Carbon/carbon composites (C/C) are also a typical fiber fabric reinforced porous composites, where synthetic pure carbon serves as the matrix, and carbon fibers are the reinforcement.<sup>3</sup> These composites have both excellent bio-inert performance of carbon materials and fine hard tissue biomechanical designability of composites.<sup>4, 5</sup> Compared with traditional medical metal and bio-ceramic materials, they possess similar elastic modulus to that of human bone. The radio-transparency of carbon element makes it easier for the doctors to evaluate the tissue reconstruction and prognosis of patients.<sup>6</sup> Besides, the porous surface texture of C/C is beneficial for obtaining a degree of bone attachment. The resulted interfacial shear strength for the C/C-bone will be obviously greater than that of the traditional titanium-bone system during the hard tissue reconstruction.<sup>7</sup>

Despite all this, previous studies indicated that the fibrous tissue formation, cartilage formation, endochondral ossifications, and intramembranous ossification appear on C/C implants simultaneously or sequentially *in vivo*.<sup>8</sup> The process embodies the typical host reaction of bioinert materials. This method of tissue reconstruction prolongs the time of post-operation recovery and increases the risk of inflammatory reaction. To solve this problem,

researchers have made use of the technologies, such as plasma spraying, chemical vapor deposition and impregnating-sintering, to prepare biomedical coatings and films, e.g., calcium phosphate/collagen,<sup>9, 10</sup> tantalum,<sup>11</sup> poly(2-hydroxyethyl methacrylate),<sup>12</sup> Ti<sub>6</sub>Al<sub>4</sub>V,<sup>13</sup> diamond-like carbon,<sup>14</sup> CNTs,<sup>15</sup> and CNTs/TiO<sub>2</sub><sup>16</sup> coatings. When the coated C/C implants are implanted into a bone as an artificial bone material, the bioactive coating can speed up the process of bio-mineralization, promotes direct osseointegration between regenerated osseous tissue and artificial bone, and consequently improves the biocompatibility of the biomedical C/C significantly. However, two outstanding problems come with the application of these technologies. Firstly, most bioactive coatings that apply to conventional metal matrixes tend to have poor wettability on the surface of C/C matrixes due to the fact that C/C are entirely composed of pure carbon. When the materials were adopted for bone tissue regeneration, the interfacial strength between the coating and the bone tissues will, during the course of coating degradation and the growth of the regenerated tissues on the coating surface, gradually surpass the coating-C/C interfacial strength. As a result, not only the material properties will undergo changes, but also the implants will become unstable in the moving system of human body.<sup>17</sup> In addition, the original porous surface structure of C/C will be changed by the biomedical coating prepared on C/C surface, thus weakening the inherent advantages of C/C as hard tissue replacement material.

Biomimetic mineralization is a method that simulates the mineralization mechanism of the natural physiological hydroxyapatite, where the bone-like calcium phosphate is deposited on the surface of the material used for repairing and replacing hard tissues so as to improve the bioactivity and bone-binding ability of the material.<sup>18, 19</sup> By mineralizing the surface of the C/C artificial bone materials, the regenerated bone-like Ca/P layer will grow on the inherent

surface of the matrix through sediment nucleation and grain aggregation. In this way, the porous feature of the original surface of C/C can be effectively retained. However, it is very hard to directly make bone-like deposits on the surface with this method because of the chemical stability of C/C, and therefore, surface pretreatment modification must be performed. For example, hydrothermal treatment of C/C with an ammonium persulfate  $[(\text{NH}_4)_2\text{S}_2\text{O}_8]$ <sup>20</sup> or  $\text{H}_2\text{O}_2$ <sup>21</sup> aqueous solutions provided surface active groups favorable for hydroxyapatite bonding to form coatings with dense morphologies and higher average shear strength. Surface modification with  $\text{H}_2\text{O}$  and  $\text{FeSO}_4$  under ultraviolet irradiation was also investigated to enhance bonding strength of hydroxyapatite coating on C/C composite.<sup>22</sup>

In the present investigation, hot nitric acid was adopted for pretreatment to generate a hydrophilic surface favorable for bonding calcium phosphate coating. Simulated body fluid immersion and electrochemical deposition were used to deposit bone-like calcium phosphate on the surface of C/C. FTIR, Raman, XPS and FE-SEM were used to analyze the changes of surface functional groups, the sediment morphology, and the deposit-matrix interfacial bonding mechanism of the post-treated C/C. In the meantime, the osseointegration property of the materials was comparatively studied by implanting them into the bones of goats.

## 2. Experimental procedure

### 2.1. Sample preparation

Polyacrylonitrile (PAN)-based C/C was prepared using chemical vapour infiltration (CVI) processing method by Yantai Luhang Carbon Materials Technology Co., Ltd in P. R. China. The density of the C/C samples is 1.6-1.7  $\text{g}/\text{cm}^3$ . C/C was machined into cubic samples of  $10 \times 10 \times 5 \text{mm}^3$  in size. After the PAN-based C/C sample was subjected to ultrasonic cleaning

with deionized water, acetone and ethanol successively, it was dried and annealed at 400°C for 2 h in an argon atmosphere. The sample was further immersed in 65% nitric acid solution at 80°C for 24 h. Finally, the sample was rinsed with deionized water and dried in vacuum at 200°C. The sample was referred as sample 1#.

Sample 1# was immersed into simulated body fluid (SBF) at 37°C.<sup>2</sup> The difference between its ion concentration and the ion concentration in human body is as shown in **Table 1**.<sup>23</sup> Then, low-frequency mechanical oscillation was applied to construct a biomimetic mineralization system. The SBF in the system was replaced once a day. The sample was taken out 21 days later, subjected to ultrasonic cleaning for 2 min, and then dried naturally at room temperature to obtain sample 2#.

**Table 1.** Ion concentrations of Kokubo solution and human blood plasma (pH=7.4)

Ion types	Na <sup>+</sup>	Cl <sup>-</sup>	HCO <sub>3</sub> <sup>-</sup>	K <sup>+</sup>	Mg <sup>2+</sup>	Ca <sup>2+</sup>	HPO <sub>4</sub> <sup>2-</sup>	SO <sub>4</sub> <sup>2-</sup>
Kokubo solution	142	147.8	4.2	5.0	1.5	2.5	1.0	0.5
Human plasma	142	103.0	27.0	5.0	1.5	2.5	1.0	0.5

In the meantime, with sample 1# used as working electrode, platinum sheet as auxiliary electrode, saturated calomel electrode as reference electrode, and SBF as electrolyte solution, electrochemical workstation (PARSTAT 2273, Princeton Applied Research Co. Ltd, USA) was used to carry out biomimetic mineralization acceleration experiment at 37±1°C for 40 min. The process parameters are as follows: working electrode potential, -1.8V; deposition current, 0.06A. Finally, after being subjected to ultrasonic cleaning for 30 s, the sample was rinsed with deionized water and dried naturally. The obtained sample is referred to as sample 3#.

## 2.2. Material characterization

Fourier transform infrared spectroscopy (FTIR, VERTEX 7, BRUKER Cooperation, Germany) was used to analyse the nature of surface functional groups of sample 1# in ATR-FTIR mode. The chemical composition of the samples was investigated by means of X-ray photoelectron spectroscopy (XPS, K-Alpha, Thermo Scientific Co.Ltd, USA) and Raman spectroscopy (LabRAM HR800 confocal Raman microscope, Horiba Scientific Co. Ltd, USA). Thermal field emission scanning electron microscopy (FE-SEM, SU-70, HITACHI Co. Ltd, Japan) equipped with Energy Dispersive Spectrometer (EDS) was adopted to characterize the surface morphology and the elementary composition of the bone-like surface of the samples. Meanwhile, the phase composition of the samples was investigated using X-ray diffractometer (XRD, XRD-6100, Shimadzu Co.Ltd, Japan), with a scan speed of 48°/min between 10 and 70° of 2 $\theta$  angles. A Cu target was used as an X-ray source using CuK $\alpha$  radiation at 40 kV and 100 mA.

## 2.3. *In vivo* test and tissue reconstruction evaluation

Two 12-month male hybrid goats were selected as animal for *in vivo* experiments. Under sterile conditions, bone defects were made at the tibial plateau. In this process, sample 3# was selected to repair the defects. The animal was kept under standard conditions in accordance with the rules for handling laboratory animals valid in the P. R. China for 90 days. Euthanasia was conducted after the prescribed period. Each implant was taken out together with the surrounding tissues. After dehydration, embedded with methyl methacrylate, the blocks of the implant with the surrounding tissues were cut into thin sections (80  $\mu$ m thick each) by LEICA sp1600 saw microtome and stained with hematoxylin and eosin (HE). Then the histological observation was carried out under an optical microscope (OM, B51, Olympus Co. Ltd, Japan).

Meanwhile, after ultrasonic cleaning, double fixed with 2.5% glutaric dialdehyde and 1% osmic acid, gradient dehydration, critical point drying and surface gold sputtering, the surface morphologies of the implants were observed to evaluate the tissue reconstruction by FE-SEM.

### 3. Results and discussion

#### 3.1. Influence of nitric acid treatment on C/C surface composition and structure

ATR-FTIR was employed to analyze the surface composition of the C/C samples before and after hot HNO<sub>3</sub> treatment (**Fig. 1**). The FTIR spectrum of the C/C sample without nitric acid treatment displays absorption peaks at 2931, 2846, 2164, 1582 and 1454 cm<sup>-1</sup> (**Fig. 1a**). The absorption peak at 2931 cm<sup>-1</sup> is attributed to C-H vibrations, while the peak at 2164 cm<sup>-1</sup> is most likely due to ketene groups. The absorption peak at 1582 cm<sup>-1</sup> corresponds to the intrinsic absorption band of graphite materials, and the absorption peak at 1454 cm<sup>-1</sup> is due to the C-H bending vibration ( $\delta_{\text{C-H}}$  in CH<sub>2</sub>). Upon treatment of the C/C sample with HNO<sub>3</sub> at 80°C for 24 h, the FTIR spectrum retained most of the original functional groups on C/C surface (**Fig. 1b**). The most salient difference between the two spectra is the appearance of relatively strong absorption peak at 3429 cm<sup>-1</sup>, indicating the formation of a large amount of hydroxyl groups on the surface of sample 1#. Meanwhile, the absorption peak at 1631 cm<sup>-1</sup> ascribed to adsorbed water on the C/C surface becomes stronger. The strong peak at 1416 cm<sup>-1</sup> can be assigned to -OH deformation vibration. From the FTIR data, we can deduce that HNO<sub>3</sub> treatment at 80°C induced C-H conversion mainly into C-OH functional groups on the C/C surface. The hydroxyl groups on the C/C surface are expected to form effective chemical bonds with -OH in HA molecules through condensation polymerization in the following processes of simulated body fluid immersion and electrochemical deposition of HA. These

treatment methods are thus believed to improve the bonding force between bone-like mineral salt deposits and C/C matrix.

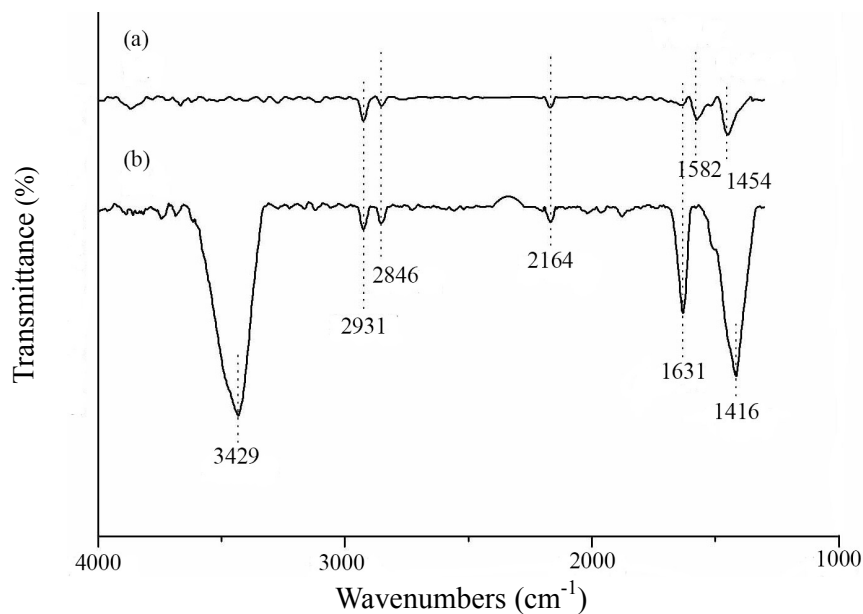


**Fig.1:** FTIR spectra of the C/C composite before (a) and after (b) nitric acid treatment (sample 1#).

Furthermore, Raman spectroscopy was used to confirm the changes occurred on the C/C before and after HNO<sub>3</sub> treatment (**Fig. 2**). The initial C/C sample displays characteristic peaks of a carbon material with two main bands located at 1360 cm<sup>-1</sup> (D band) and 1580 cm<sup>-1</sup> (G band) with I<sub>D</sub>/I<sub>G</sub> ratio of 0.81.<sup>24</sup> The D band is attributed to in-plane disorder in the graphitic structure, while the G band is associated with the level of graphitization. There are no obvious changes in the Raman spectrum of the HNO<sub>3</sub>-treated sample (sample 1#). However, a significant increase of the I<sub>D</sub>/I<sub>G</sub> ratio (1.28) is observed, indicating an increase of disorder in the graphitic structure.

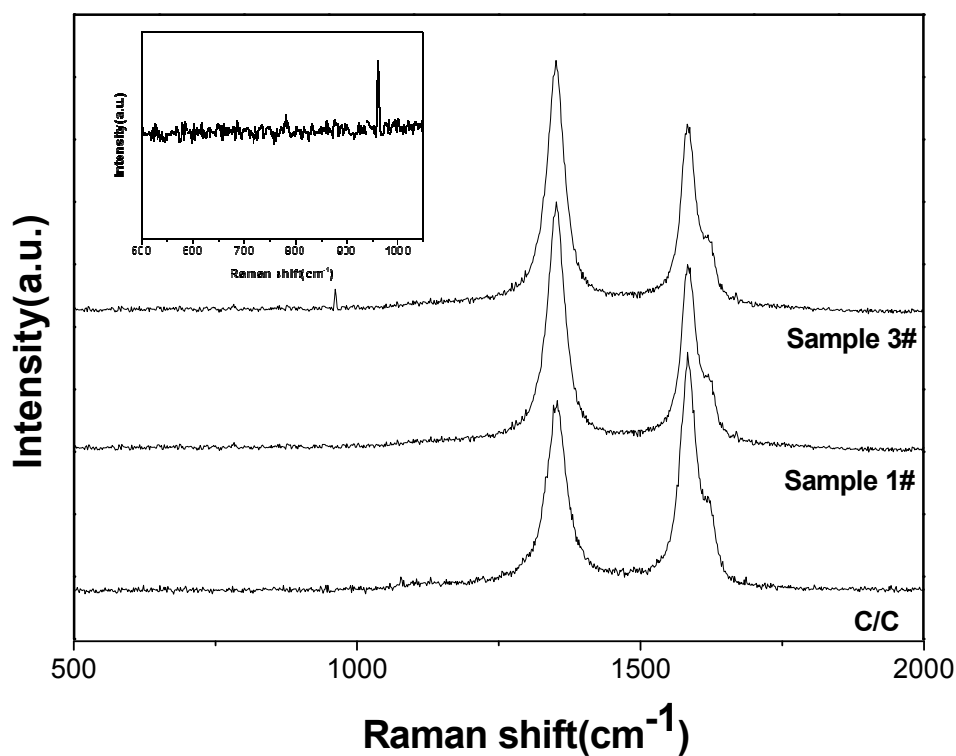


**Fig.2:** Raman spectra of the C/C composite before and after nitric acid treatment (sample 1#), and after HAP deposition (sample 3#). The inset corresponds to the symmetric stretching mode ( $\nu_3$ ) of phosphate ion in HAp.

X-ray photoelectron spectroscopy (XPS) analysis of the C/C composite shows a main peak at 285.0 eV due to  $C_{1s}$  and a small peak at 531.8 eV assigned to  $O_{1s}$ . The latter may result from partial surface oxidation or from of organic contamination during sample handling and storage (**Fig. 3**). The oxygen atomic concentration in the C/C sample is 5.54% (**Table 2**). After  $HNO_3$  treatment, a significant increase of the  $O_{1s}$  atomic concentration is observed (9.18%), in agreement with surface oxidation of the sample. The slight increase of the  $N_{1s}$  atomic concentration in the sample1# is most likely due residual  $HNO_3$ .

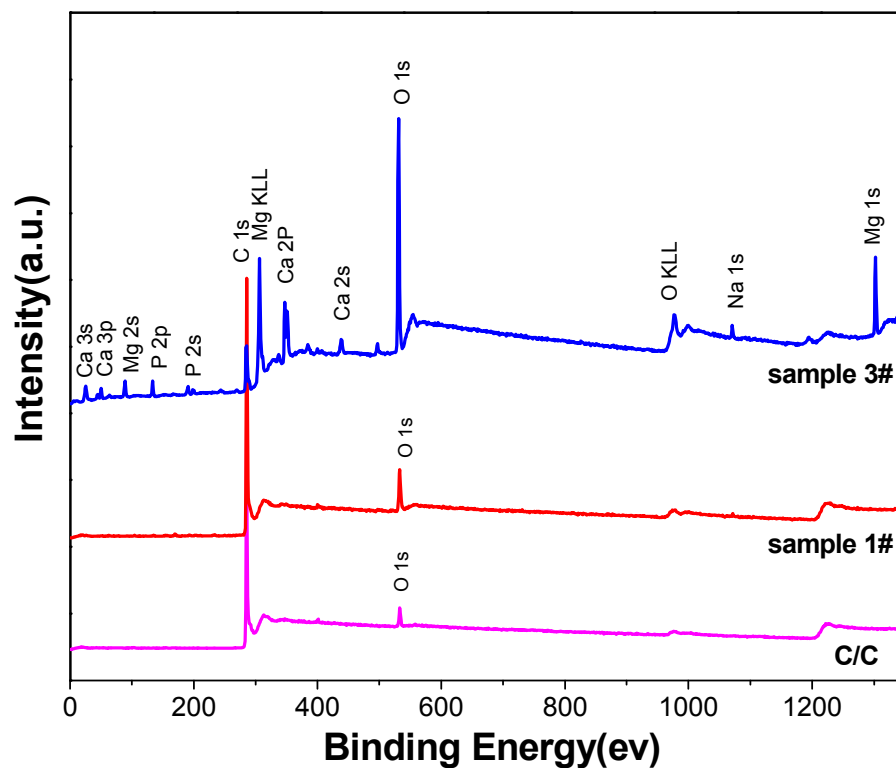


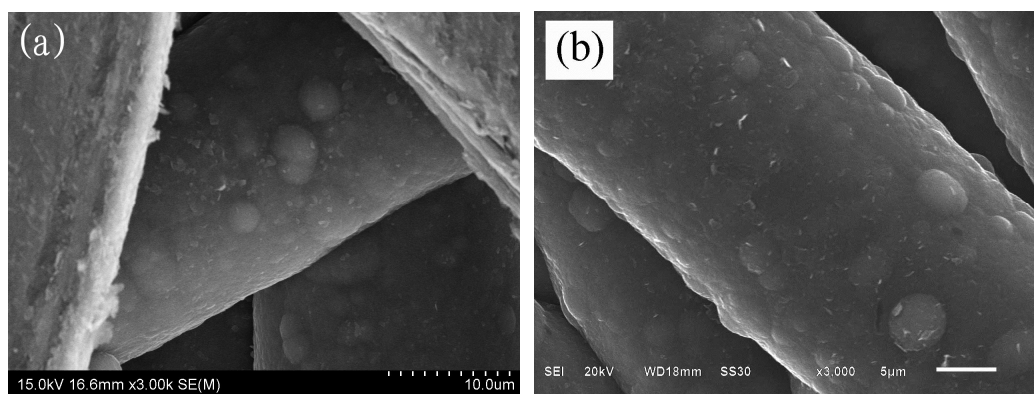
**Fig.3:** XPS survey spectra of the C/C composite before and after nitric acid treatment (sample 1#), and after HAp deposition (sample 3#).

**Table 2.** Element composition of the samples

Sample	Atomic percentage%					
	C	O	N	Ca	P	Mg
C/C	93.27	5.54	1.19	0	0	0
Sample1#	89.03	9.18	1.79	0	0	0
Sample3#	28.91	45.9	3.07	9.23	5.15	7.74

**Fig. 4** shows the morphology of the C/C sample before and after  $\text{HNO}_3$  treatment observed by means of FE-SEM. Since the samples had been subjected to ultrasonic cleaning in various media, the sample surface mainly took the form of carbon fiber braids. **Fig. 4a** displays the FE-SEM image of the C/C sample without nitric acid treatment; there are many hemispherical bulges on the carbon fiber surface, which are traces left by gaseous by-products and damping gases when escaping from the inclusions of the surface of carbon fibers. These gaseous

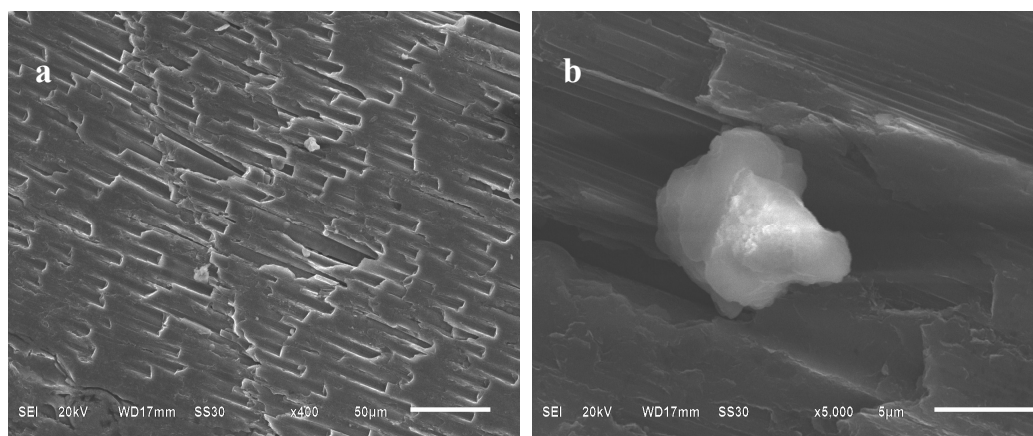
by-products and damping gases are generated by the pyrolysis of PAN residual in carbon source gases or fibers during the preparation of C/C with CVD method as well as the follow-up carbonization and graphite heat treatment processes. **Fig. 4b** exhibits the micro-morphology of the C/C surface that has been subjected to HNO<sub>3</sub> treatment at 80°C for 24 h at the same magnification. Through comparison, no significant change was observed in the carbon fiber structure of C/C or the micro-morphology of the carbon fibers before and after nitric acid treatment.



**Fig. 4:** FESEM morphologies of the C/C composite before (a) and after (b) nitric acid treatment (sample 1#).

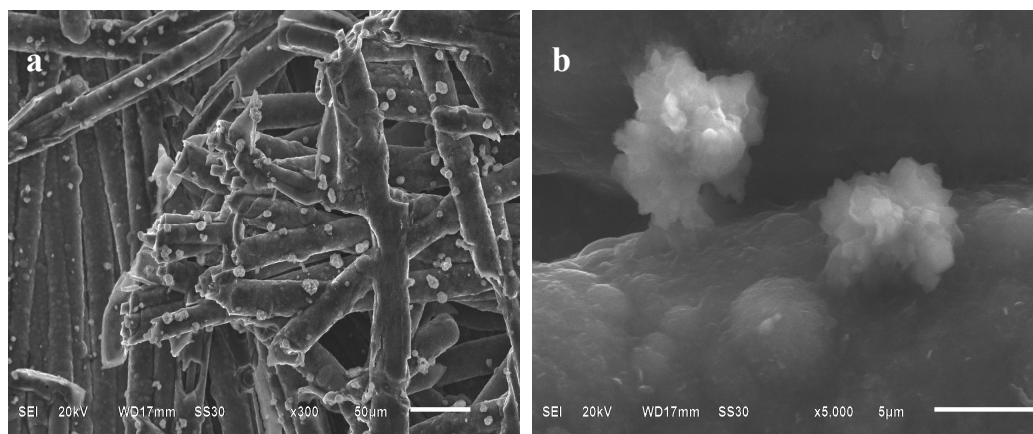
### 3.2. Surface structure and mechanism analysis of biomimetic mineralization samples

**Fig. 5** depicts the SEM images of pure C/C after 21 days immersion in SBF. One clearly sees that the surface morphology has typical C/C structure with barely any deposit (**Fig. 5a**). At higher magnification (5000X), a small amount of white crystals embedded within the grooves of carbon fibers, corresponding most likely to SBF precipitants generated during the immersion process, were observed (**Fig. 5b**).



**Fig. 5:** SEM images of non pretreated C/C samples soaked in SBF for 21 days  
a) 400 $\times$ , b) 5000 $\times$

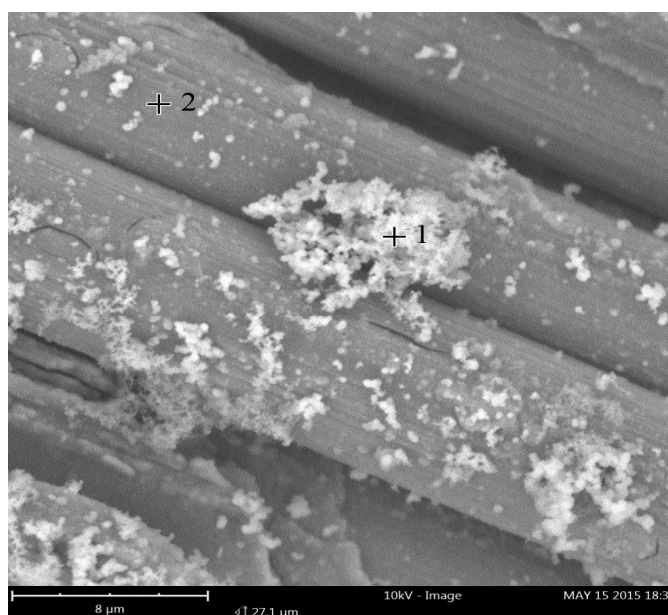
These white crystals were retained by the grooves on the C/C surface even after ultrasonic cleaning step. However, they actually did not bind to the C/C surface nor did they change the surface structure. **Fig. 6** depicts the SEM images of the HNO<sub>3</sub>-treated sample upon immersion in SBF for 21 days (sample 2#). In contrast to the non-treated sample, a large amount of deposits with aggregate morphology was formed on the surface of carbon fibers (**Fig. 6a**).



**Fig. 6:** SEM images of sample 2# soaked in SBF for 21 days a) 300 $\times$ , b) 5000 $\times$

At higher magnification (5000X), these deposits, about 5  $\mu\text{m}$  in size, consisted of spherical or flaky small particles distributed evenly on the surface of the carbon fibers. The tight bonding formed between the deposits and the carbon survived the ultrasonic cleaning with various media, and a “bridging” connection was formed on the interface. This is because the original

C-H on the surface of carbon fibers were converted into C-OH under the effect of concentrated nitric acid, and the follow-up SBF immersion enabled the molecules of the bone-like Ca/P layer to form effective chemical bonding on the surface of the carbon fibers through condensation polymerization, with the -OH on the C/C surface serving as the nucleation sites. Ultimately, the C/C surface structure with optimized biological activity was obtained. EDS and XRD were employed to determine the chemical components and structure of the deposits. **Fig. 7** exhibits the SEM image of the sample 2#. It shows that the surface deposits existed in the form of spherical particle aggregates, all of which are uniform in size of about 100 nm. The element analysis revealed that at the initial nucleation period of the deposits, SBF elements, such as Ca, P, O, Mg and Na, were uniformly distributed on the surface of the carbon as ions, and the deposits covered the surface of the carbon fibers in the form of homogeneous nucleation. Afterwards, the particles with inhomogeneous nucleation formed loosely-structured aggregates on the surface of the material to constitute the as-deposited bone-like deposit layer. **Fig. 8** schematically depicts the different steps and plausible mechanism of biomimetic mineralization.



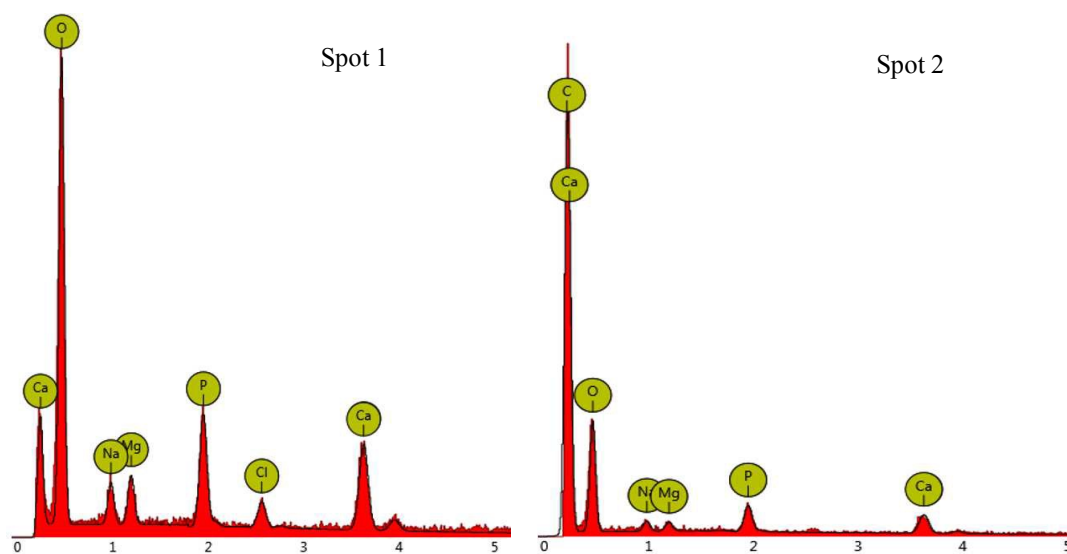


**Fig. 7:** SEM image and EDS spectra of sample 2# recorded at two different spots on the surface.

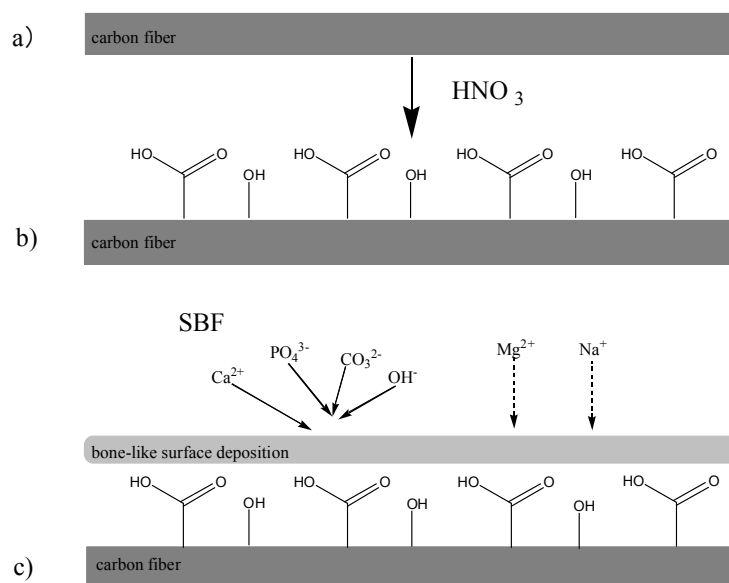


**Fig. 8:** Schematic view of the biomimetic mineralization steps and formation of bone-like layers on C/C substrates: (a) initial C/C surface, (b) formation of functional groups on the carbon fiber through oxidation with HNO<sub>3</sub> solution, (c) deposition nucleation and layer formation through absorbing Ca<sup>2+</sup>, PO<sub>4</sub><sup>3-</sup>, Mg<sup>2+</sup>, Na<sup>+</sup> and CO<sub>3</sub><sup>2-</sup> from SBF.

XRD analysis revealed that the deposits were mainly composed of hydroxyapatites (HAp). After immersion in SBF for 21 days, the formation of HAp on hydroxyl-modified carbon fibers was clearly evidenced through pronounced signals at  $2\theta=26.0^\circ$ ,  $32.2^\circ$  and  $53.8^\circ$

according to ICDD PDF 2, pattern 54-0022. The above three apparent X-ray diffraction peaks correspond to the three crystal faces of HAp i.e. (002), (112) and (004), respectively (**Fig. 9**). By means of the well-known Scherrer formula, the average crystallite size  $L_{hkl}$  for (hkl) direction can be calculated as follows:<sup>25</sup>

$$L_{HKL} = K \lambda / \beta_{HKL} \cos \theta$$

where  $K$ ,  $\theta$ ,  $\lambda$  and  $\beta_{HKL}$  respectively represent the shape factor, diffraction angle, the wavelength of the X-rays, and the full width at half maximum from the (hkl) peak. For HAp deposited on sample 2#, the calculated results indicate that the crystallite size  $L_{112}$  is 15.5 nm. This shows that the surface deposits on sample 2# are Mg and Na iron-doped nano-HAp. Through chemical reactions such as esterification and condensation, the nano-HAp particles form chemical bonding with hydroxylated carbon fibers. This indicates that the hydroxylated composite biomimetic mineralization technology has solved the problem of poor bonding performance of conventional bioactive coatings due to poor wettability of pure carbon materials. It is reported that magnesium is a minor but important component of bone, enamel and dentine and it plays an essential role in the bio-mineralization process.<sup>26, 27</sup> Compared with pure HAp of the same crystallinity, the bone implant material of Mg-doped HAp has significantly higher adhesion and proliferation on the surface of osteoblast cells. Therefore, HAp has better osteoconductivity and it can promote cellular functions and biocompatibility.<sup>28</sup>

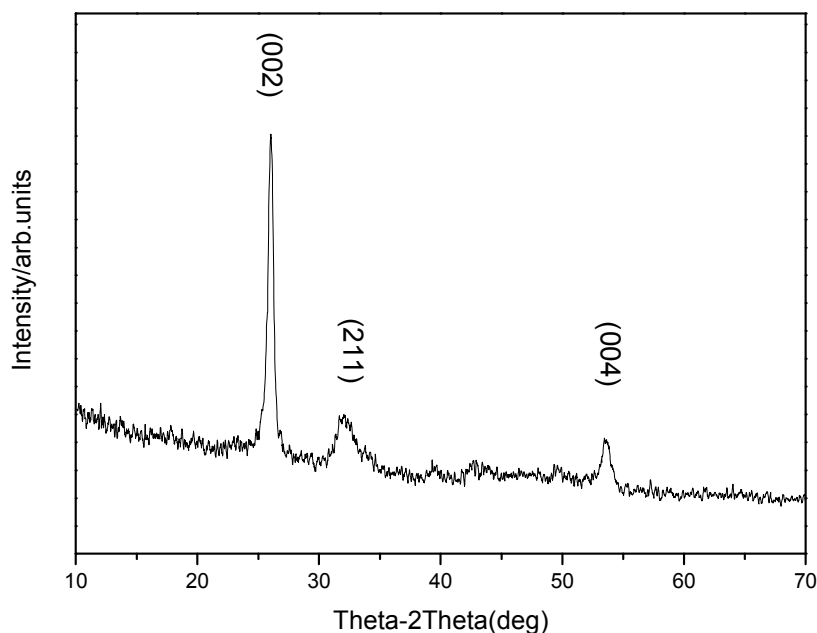


**Fig. 9:** XRD spectrum of sample 2# confirming the formation of HAp.

The results of the experiments show that HAp deposits that can form tight bonding with carbon fibers can be obtained by means of SBF biomimetic mineralization on  $\text{HNO}_3$ -pretreated C/C samples. It is expected that this new C/C surface structure will have excellent bone tissue compatibility and thus great potential in the application of bone tissue scaffold.<sup>29</sup> However, this treatment process requires a long time. To speed up this process, we introduced an electrochemical method. As shown in **Fig. 10**, there are large amounts of spherical particles on the surface of sample 3#. At higher magnification, it can be seen that the morphology, aggregate structure and size of these particles highly resembled those of the deposits on the surface of sample 2#, and they had also formed “bridging” connection with the carbon fibers. By means of XRD analysis, the deposits were mainly composed of HAp crystals (**Fig. 11**), just like the deposits on sample 2#. These results are corroborated by Raman and XPS results. Indeed, the presence of a very sharp peak at  $961\text{ cm}^{-1}$  in the Raman spectrum of sample 3#, due to symmetric stretching mode ( $\nu_3$ ) of phosphate ion,<sup>30</sup> is a good

indication of HAp deposition on the surface (**Fig. 2**). Also XPS analysis of sample 3# shows additional peaks due to Mg, Ca and P (**Fig. 3**), which are absent in sample 1# and a huge increase of the O<sub>1s</sub> atomic concentration (**Table 2**).

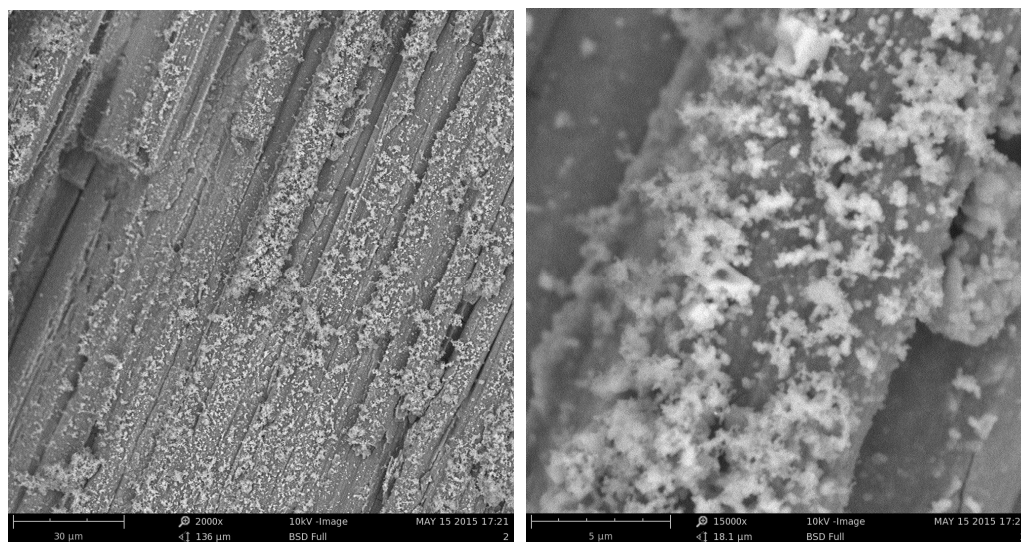


**Fig. 10:** SEM images of sample 3#: a) 2000×; b) 15000×

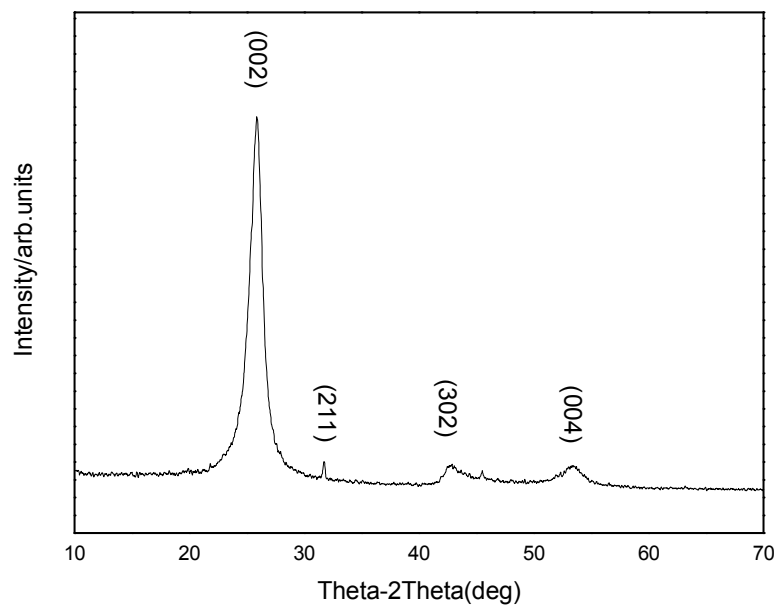


**Fig. 11:** XRD spectrum of sample 3# confirming the formation of HAp.

### 3.3. *In vivo* tissue reconstruction on the interface between C/C implants and bone tissue

Two 12-month male hybrid goats were selected as animal for *in vivo* experiments. Under

sterile conditions, bone defects were made at the tibial plateau. In this process, sample 3# was selected to repair the defects. Within 90 days after the implantation, all daily physiological indexes such as breath, cardiac rate and body temperatures were all within the normal range.

**Fig. 12** shows the HE stained histological cross-sections of the tissue around the implants at day 90. From the near to the distant, newborn bone trabecula, cartilage tissue and bone marrow appear on the interface between C/C implants and bone tissue. In newborn bone trabecula, there exists a Haversian system with complete morphology, indicating a well-developed regenerated bone tissue. No lymph node hyperplasia and inflammatory cell infiltration was detected. This highly resembles the morphology of the bone tissue reconstructed on the surface of HAp coating that was previously prepared on the C/C surface by means of plasma spraying,<sup>6, 8</sup> but a striking difference was observed compared with that on pure C/C surface with typical biological inert characteristics as studied before.<sup>31</sup> The regenerated bone tissues on the surface of sample 3# were directly bound with the material in the Ca, Ma and PO<sub>4</sub> rich environment provided by degraded HAp. The data indicates that sample3# has excellent bone tissue compatibility. In addition, there were no dissociated carbon particles in the tissues surrounding the implant nor was any macrophage detected, suggesting that the chemical state on the surface of the material was improved significantly.

**Fig. 13** displays a characteristic SEM image of the surface of the implants at day 90. It shows attached osteoblasts which begun to spread on the carbon fiber of the implant. The cells were covered by a dense coating matrix and were able to migrate throughout the implant. The surface of the implant exhibited a thin layer of extracellular matrix. We also found that the cells did not adhere closely to the smooth surface of the carbon fibers. Meanwhile, the cells tend to proliferate in the porous structure on the implant surface. These results are in

agreement with previous reports,<sup>32, 33</sup> where it has been established the influence of the surface topography on cell attachment. In this sense, it is very useful to retain the porous structure of the original C/C surface during the surface modification of biomimetic mineralization as illustrated in this study.

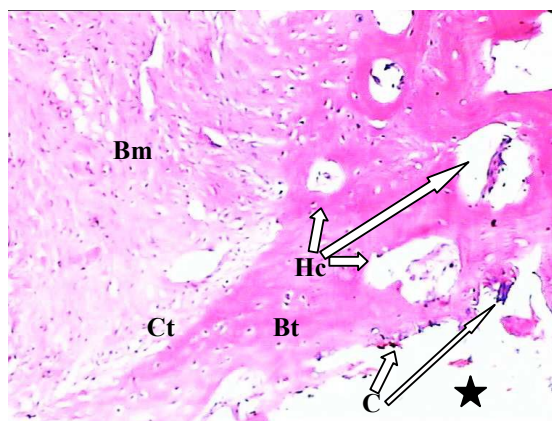


**Fig. 12:** HE stained histological cross-sections of the tissue around the implants at day 90. Bt: bone trabecula; Ct: cartilage tissue; Bm: bone marrow tissue; Hc: Halverson canal; C: carbon particle; ★ : the position of implant.

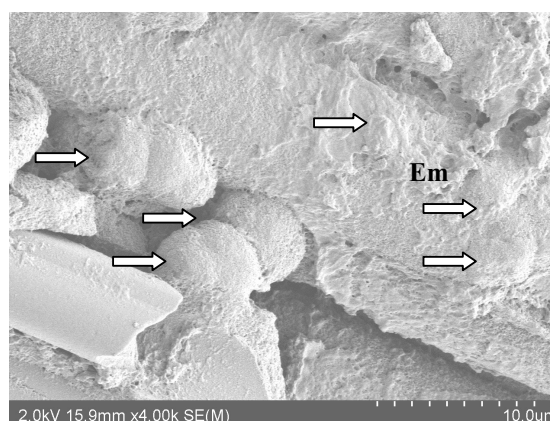


**Fig. 13:** SEM image of the implant surface at day 90. Arrows show osteoblasts; Em: extracellular matrix

## Conclusion

We have demonstrated that by a simple HNO<sub>3</sub> treatment, the C/C composite surface can be turned from inert to bioactive through generation of a hydroxyl-terminated surface. By means of biomimetic mineralization, Mg-doped HAp particles were successfully deposited on the hydroxyl-modified C/C surfaces through chemical bonding. The original porous morphology of the C/C surface, essential to cell proliferation, was well preserved during the process. Meanwhile, introduction of an electrochemical method for HAp deposition sped up the mineralization process and helped to build a bone-like surface layer. 90 days after the implantation for bone defect repair, the implants perfectly fulfilled their mission. The tissue reconstruction of the bone defect area was completed without any toxicity and inflammation. The surface of this kind of C/C based biomaterials was not only directly connected to

newborn bone tissues compared with bioinert pure C/C, but also exhibited excellent surface chemical stability compared with existing plasma-sprayed HAp coated C/C. Due to the osteoconductive effect of the materials, the bone defect healing process was sped up and the surface bioactivity of C/C implant was substantially improved. In this sense the materials organically integrate the biomechanical properties and surface biological activity of C/C.

### Acknowledgements

This work was supported by the National Natural Science Foundation of China with grant No. 51302320, No.81503594 and the Fundamental Research Funds for the Central Universities of P. R. China with grant No. 14CX02200A and No.14CX05094A.

### References

- <sup>1</sup> B. Clark, *Clinic J. Am. Soc. Nephrology*, 2008, **3**, S131.
- <sup>2</sup> S. Weiner and P. M. Dove, *Rev. Mineral. Geochem.*, 2003, **54**, 1.
- <sup>3</sup> J. E. Sheehan, K. W. Buesking, and B. J. Sullivan, *Annu. Rev. Mater. Sci.*, 1994, **24**, 19.
- <sup>4</sup> N. Cao, Q. X. Wang, J. W. Dong, G. Z. Hao, and M. S. Li, *New Carbon Mater.*, 2010, **25**, 232.
- <sup>5</sup> G. H. Wang, S. Yu, S. H. Zhu, C. Q. Gao, Y. Liu, Y. L. Miu, and B. Y. Huang, *J. Mater. Sci.: Mater. Med.*, 2009, **20**, 2487.
- <sup>6</sup> N. Cao, J. W. Dong, Q. X. Wang, Q. S. Ma, C. Q. Xue, and M. S. Li, *Surf. Coat. Technol.*, 2010, **205**, 1150.
- <sup>7</sup> D. Adams and D. F. Williams, *Biomaterials*, 1984, **5**, 59.

- <sup>8</sup> N. Cao, J. W. Dong, Q. X. Wang, Q. S. Ma, F. Wang, H. Y. Chen, C. Q. Xue, and M. S. Li, *J. Biomed. Mater. Res. A*, 2010, **92A**, 1019.
- <sup>9</sup> X. N. Zhao, T. Hu, H. J. Li, M. D. Chen, S. Cao, L. L. Zhang, and X. H. Hou, *Appl. Surf. Sci.*, 2011, **257**, 3612.
- <sup>10</sup> X. N. Zhao, H. J. Li, M. D. Chen, K. Z. Li, B. Wang, Z. W. Xu, S. Cao, L. L. Zhang, H. L. Deng, and J. H. Lu, *Appl. Surf. Sci.*, 2012, **258**, 5117.
- <sup>11</sup> H. Li, X. Zou, C. Woo, M. Ding, M. Lind, and C. Bunger, *J. Biomed. Mater. Res. B*, 2007, **81B**, 194.
- <sup>12</sup> V. Pesakova, K. J. Smetana, M. Sochor, H. Hulejova, and K. Balik, *J. Mater. Sci.: Mater. Med.*, 2005, **16**, 143.
- <sup>13</sup> L. L. Zhang, H. J. Li, J. H. Lu, Y. L. Zhang, S. Cao, X. N. Zhao, and Z. B. He, *Surf. Interface Anal.*, 2013, **45**, 973.
- <sup>14</sup> D. Devlin, J. Cowie, D. Carroll, and D. Rivero, *Proc. 1995 ASME Int. Mech. Eng. Congress Exposition, San Francisco, USA, Nov 12-17, 1995:31-32*.
- <sup>15</sup> W. J. Lee, D. H. Lee, T. H. Han, S. H. Lee, H.-S. Moon, J. A. Lee, and S. O. Kim, *Chem. Commun.*, 2011, **47**, 535.
- <sup>16</sup> W. J. Lee, J. M. Lee, S. T. Kochuveedu, T. H. Han, H. Y. Jeong, M. Park, J. M. Yun, J. Kwon, K. No, D. H. Kim, and S. O. Kim, *ACS Nano*, 2012, **6**, 935.
- <sup>17</sup> B. Sebok, G. Kiss, P. J. Szabo, D. Rigler, M. L. Molnar, G. Dobos, F. Reti, H. Szocs, A. F. Joob, S. Bogdan, and G. Szabo, *J. Mater. Sci.: Mater Med*, 2013, **24**, 821.
- <sup>18</sup> A. Hoppe, J. Will, R. Detsch, A. R. Boccaccini, and P. Greil, *J. Biomed. Mater. Res. A*, 2014, **102A**, 193.
- <sup>19</sup> G. Chatelain, D. Bourgeois, J. Ravaux, O. Averseng, C. Vidaud, and D. Meyer,

- Biomed. Mater.*, 2014, **9**, 1.
- 20 X.-b. Xiong, X.-r. Zeng, C.-L. Zou, and J.-Z. Zhou, *Acta Biomater.*, 2009, **5**, 1785.
- 21 X.-b. Xiong, X.-r. Zeng, and C.-L. Zou, *Mater. Chem. Phys.*, 2009, **114**, 434.
- 22 Z. Leilei, L. Hejun, S. Qiang, L. Kezhi, L. Jinhua, L. Wei, S. Mikhalovsky, and C. Sheng, *Surf. Rev. Lett.*, 2014, **21**, 1450016.
- 23 T. Kokubo and H. Takadama, *Biomaterials*, 2006, **15**, 2907.
- 24 Z. Leilei, L. Hejun, S. Qiang, L. Kezhi, L. Jinhua, L. Wei, S. Mikhalovsky, and C. Sheng, *Surf. Rev. Lett.*, 2014, **21**, 1450016.
- 25 S. N. Danilchenko, O. G. Kukhareno, C. Moseke, I. Y. Protsenko, L. F. Sukhodub, and B. S. Cleff, *Cryst. Res. Technol.*, 2002, **37**, 1234.
- 26 S. Pina, S. Olhero, S. Gheduzzi, A. Miles, and J. Ferreira, *Acta Biomater.*, 2009, **5**, 1233.
- 27 A. Zima, Z. Paszkiewicz, D. Siek, J. Czechowska, and A. Slosarczyk, *Ceram. Inter.*, 2012 **38**, 4935.
- 28 W. Mroz, A. Bombalska, S. Burdynska, M. Jedynski, A. Prokopiuk, B. Budner, A. Slosarczyk, A. Zima, E. Menaszek, A. Scislowska-Czarnecka, and K. Niedzielski, *J. Mol. Struct.*, 2010, **977**, 145.
- 29 J. H. Wang, Z. F. Ouyang, Z. W. Ren, J. F. Li, P. P. Zhang, G. Wei, and Z. Q. Su, *Carbon*, 2015, **89**, 20.
- 30 D. Yamini, G. Devanand Venkatasubbu, J. Kumar, and V. Ramakrishnan, *Spectrochim. Acta A*, 2014, **117**, 299.
- 31 N. Cao, J. W. Dong, and W. B. Wang, *J. Shanghai Jiaotong University*, 2012, **17**, 537.
- 32 Z. A. Bakar, B. F. Hussein, and N. M. Mustapha, in 'Cockle Shell-Based

Biocomposite Scaffold for Bone Tissue Engineering, Regenerative Medicine and Tissue Engineering-Cells and Biomaterials', ed. D. Eberli, 2011.

- <sup>33</sup> J. M. Sautier, J. R. Nefussi, H. Boulekbache, and N. Forest, *In Vitro Cell. Dev. Biol.*, 1990, **26**, 1079.

By means of biomimetic mineralization method, Mg-doped hydroxyapatite nano particles were successfully prepared on hydroxyl-modified C/C surfaces.

